A NEW APPROACH TO THE EXPERIMENTAL DETERMINATION OF THE DYNAMIC STRESS INTENSITY FACTOR

H. D. Bui†, H. Maigre and D. Rittel
Laboratoire de Mecanique des Solides, U.R.A. 317-C.N.R.S., Ecole Polytechnique, F-91128
Palaiseau Cedex, France

Abstract—This paper addresses the determination of the evolution of the dynamic stress intensity factor $KI_d(t)$ for a non-propagating crack subjected to transient loading. A new and rigorous approach is presented in its theoretical and experimental aspects. First, for linear-elastic materials it is shown that crack-tip singularities are related to global mechanical parameters (forces-displacements on the boundaries of the structure) through the path-independent H-integral which includes dynamic effects. KId (t) is thus determined by solving a time convolution equation. Practical implementation of the method is then illustrated by a simple and original experimental procedure together with its numerical simulation. Experimental and numerical results are finally used to validate the feasibility and efficiency of the proposed method.

1. INTRODUCTION

When a cracked structure is subjected to dynamic loading, it is important to determine the corresponding stress intensity factor as a first step towards fracture prediction. Practical aspects of the problem involve actual structures and materials subjected to arbitrary dynamic loads. The problem addressed here is that of the determination of the evolution of the dynamic stress intensity factor $K_{Id}(t)$ from the very beginning of the loading.

Different types of approaches are currently available. The first type is based on an extension of static results [e.g. Rice's J-integral (1968)] for the dynamic case. Such an approach is not supported by theoretical arguments and it can sometimes lead to totally erroneous results (Mall *et al.,* 1980). Much better results are obtained with the second type of approach of a hybrid experimental-numerical character (Yang *et al.,* 1988). Here, each experiment must be numerically simulated including crack propagation aspects. Another type of approach is based on direct observations of crack-tip phenomena, such as light reflection (or transmission) in the so-called method of caustics (Manogg, 1966; Beinert and Kalthoff, 1981; Theocaris, 1981). Here, a relationship is derived between the shadow pattern (shape and characteristic size) and the crack-opening mode and stress intensity factors. Other modern methods have been reviewed by Kobayashi (1987). However, each method has its own limitations either in its accuracy or because of the experimental difficulties encountered.

Therefore, the main objective of this paper is to treat the crack's history from the onset of loading until its very early propagation without addressing propagation aspects. We present an exact approach which is both accurate and relatively easy to implement in the laboratory. This approach is based on a theoretical method for the determination of the dynamic stress intensity factor given by Bui and Maigre (1988), Maigre (1990) (Section 2), including its experimental implementation (Sections 3 and 4) and validation (Sections 5 and 6).

† Electricité de France, D.E.R., F-92141 Clamart Cedex, France.

2. PATH-INDEPENDENT *H*-INTEGRAL

Let Ω be a two-dimensional body with a crack of length a laying parallel to x_1-axis, as shown in Fig. 1. The solid is linear-elastic, isotropic and homogeneous; p, E and v denote mass density, Young's modulus and Poisson's ratio, respectively. The geometry and dynamic loads are symmetrical with respect to x_1-axis to consider fracture in pure mode I. Let $\mathbf{u}(\mathbf{x}, t; a)$ denote a displacement field on Ω. The load $\mathbf{T}[\mathbf{u}]$ is applied on the boundary S and depends on time $t \geq 0$. The body is initially at rest so that $\mathbf{u}$ satisfies

$$\begin{cases} \mathbf{u}(t \leqslant 0) = 0, \\ \dot{\mathbf{u}}(t \leqslant 0) = 0. \end{cases} \tag{1}$$

The superscript (·) indicates time derivative.

Next, define an adjoint field, $\mathbf{V}(\mathbf{x}, t; a, \tau)$ on Ω such that

$$\begin{cases} \mathbf{V}(t \geqslant \tau) = 0, \\ \dot{\mathbf{V}}(t \geqslant \tau) = 0. \end{cases} \tag{2}$$

$\mathbf{u}$ and $\mathbf{V}$ are solutions of the dynamic equations:

$$\text{div } \boldsymbol{\sigma}[\mathbf{u}] = \rho \frac{\partial \dot{\mathbf{u}}}{\partial t}, \tag{3}$$

$$\text{div } \boldsymbol{\sigma}[\mathbf{V}] = \rho \frac{\partial \dot{\mathbf{V}}}{\partial t}, \tag{4}$$

where $\boldsymbol{\sigma}[\mathbf{u}] = 1/2\mathbf{L}(\nabla\mathbf{u} + ^T\nabla \mathbf{u})$ is the elastic stress tensor associated with $\mathbf{u}$ and $\mathbf{L}$ denotes the tensor of elastic moduli.

Note that a and τ are parameters which are held constant during the dynamic deformation of Ω. $\mathbf{V}$ is an auxiliary field which satisfies (4) and is subjected to (2). It should be remarked that $\mathbf{V}$ does not necessarily represent a *physical* field (e.g. displacement). Rather,
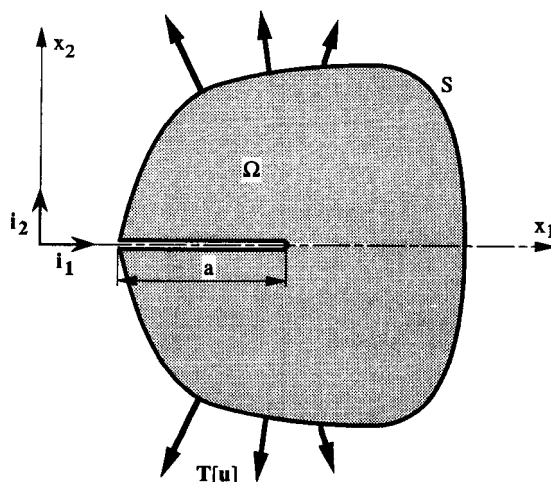

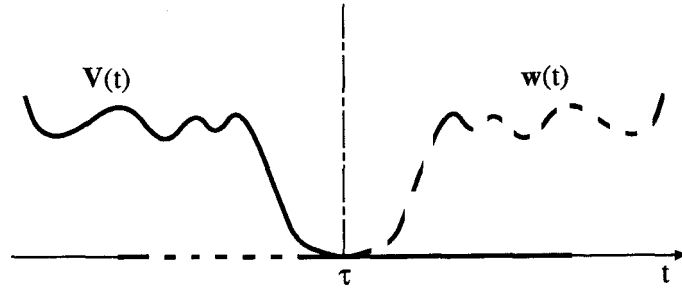Fig. l. Cracked body loaded in mode I.

Fig. 2. Schematic representation of the auxiliary field **V** as a "mirror image" of a physical field **w** at fixed **x**.

as shown in Fig. 2, **V** is a "mirror image" with respect to time $t = \tau$ of some physical dynamic field, say **w**(**x**, t) at rest at $t \leq \tau$.

Next, eqns (3) and (4) are combined to yield the following conservation law:

$$\operatorname{div}\left\{\boldsymbol{\sigma}[\mathbf{u}]\cdot\mathbf{V}-\boldsymbol{\sigma}[\mathbf{V}]\cdot\mathbf{u}\right\} = \rho\frac{\partial(\mathbf{V}\cdot\dot{\mathbf{u}}-\mathbf{u}\cdot\dot{\mathbf{V}})}{\partial t}. \tag{5}$$

By integrating (5) in the time limits 0-τ the right-hand side vanishes because of the initial conditions for **u** and the final conditions for **V**, (1) and (2), i.e.

$$\operatorname{div}\int_0^\tau\left\{\boldsymbol{\sigma}[\mathbf{u}]\cdot\mathbf{V}-\boldsymbol{\sigma}[\mathbf{V}]\cdot\mathbf{u}\right\}\mathrm{d}t = 0. \tag{6}$$

Equation (6) is valid for all points of Ω with the possible exception of the crack-tip where the fields are likely to be singular. Therefore, we integrate (6) on the domain Ω with the exclusion of Ω_Γ which is part of Ω delimited by the curve Γ surrounding the crack-tip (Fig. 3). The result is the following expression, invariant with respect to Γ:

$$\int_{\Omega-\Omega_\Gamma}\left[\operatorname{div}\int_0^\tau\left\{\boldsymbol{\sigma}[\mathbf{u}]\cdot\mathbf{V}-\boldsymbol{\sigma}[\mathbf{V}]\cdot\mathbf{u}\right\}\mathrm{d}t\right]\mathrm{d}\Omega = 0, \quad \forall\,\Gamma. \tag{7}$$

Upon integration of (7) by parts, it appears that

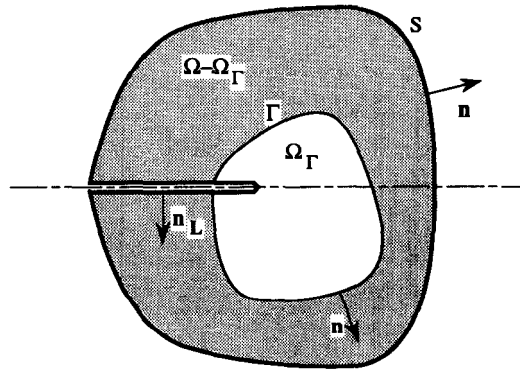Fig. 3. The integration domain.

$$\int_{\Gamma} \mathbf{n} \cdot \int_0^{\tau} \{\boldsymbol{\sigma}[\mathbf{u}] \cdot \mathbf{V} - \boldsymbol{\sigma}[\mathbf{V}] \cdot \mathbf{u}\} \, \mathrm{d}t \, \mathrm{d}\Gamma - \int_S \mathbf{n} \cdot \int_0^{\tau} \{\boldsymbol{\sigma}[\mathbf{u}] \cdot \mathbf{V} - \boldsymbol{\sigma}[\mathbf{V}] \cdot \mathbf{u}\} \, \mathrm{d}t \, \mathrm{d}S$$

$$= \int_L \mathbf{n}_L \cdot \int_0^{\tau} \{\boldsymbol{\sigma}[\mathbf{u}] \cdot \mathbf{V} - \boldsymbol{\sigma}[\mathbf{V}] \cdot \mathbf{u}\} \, \mathrm{d}t \, \mathrm{d}L, \quad \forall \, \Gamma, \quad (8)$$

where n and n_L are normal unit vectors as shown in Fig. 3. The right-hand side of (8) equals zero because the crack faces are traction-free. It can thus be seen that the leftmost term of (8) is independent of F. Consequently, the path-independent integral $H(\tau)$ is defined as follows (Bui and Maigre, 1988; Maigre, 1990)

$$H(\tau) = \frac{1}{2} \int_{\Gamma} \int_0^{\tau} \{\mathbf{n} \cdot \boldsymbol{\sigma}[\mathbf{u}] \cdot \mathbf{V} - \mathbf{n} \cdot \boldsymbol{\sigma}[\mathbf{V}] \cdot \mathbf{u}\} \, \mathrm{d}t \, \mathrm{d}\Gamma, \quad \forall \, \Gamma. \tag{9}$$

Note that $H(\tau)$ is not only path-independent but it is also a pure contour integral. Among the possible integration paths, it is particularly attractive to evaluate $H(\tau)$ on the boundary S where forces $\mathbf{T}[\mathbf{u}] = \mathbf{n} \cdot \boldsymbol{\sigma}[\mathbf{u}]$ and displacements $\mathbf{u}$ can be experimentally measured :

$$H(\tau) = \frac{1}{2} \int_S \int_0^{\tau} \{\mathbf{T}[\mathbf{u}] \cdot \mathbf{V} - \mathbf{T}[\mathbf{V}] \cdot \mathbf{u}\} \, \mathrm{d}t \, \mathrm{d}S. \tag{10}$$

Another interesting integration path is that obtained by letting Γ shrink close to the crack-tip itself.

In order to have a non-vanishing result for $H(\tau)$, the integrand of (9) must necessarily vary as $1/r$ where r is the distance from the crack-tip ($r = |\mathbf{x} - a\mathbf{i}_1|$). The displacement field $\mathbf{u}$ is known to vary asymptotically as $r^{1/2}$ and the stress field $\boldsymbol{\sigma}[\mathbf{u}]$ as $r^{1/2}$ when r tends to 0. Consequently, the adjoint quantity $\mathbf{V}(\mathbf{x})$ must vary as $r^{1/2}$. To build such a field, we use an auxiliary displacement field $\mathbf{v}(\mathbf{x}, t; a)$ which satisfies initial conditions (1) like $\mathbf{u}$ and varies as $r^{1/2}$. We define $\mathbf{V}$ as

$$\mathbf{V}(\mathbf{x}, t; a, \tau) = \frac{\partial \mathbf{v}(\mathbf{x}, \tau - t; a)}{\partial a}. \tag{11}$$

It is worth noting that with this definition, $\mathbf{V}$ satisfies not only the final conditions (2) but also (4) because the latter is not affected by an inversion of the time flow.

In the vicinity of the crack-tip, $\mathbf{u}$ and $\mathbf{V}$ are totally defined as function of K_{Id}^u and K_{Id}^v, the dynamic stress intensity factors associated with $\mathbf{u}$ and $\mathbf{v}$ respectively. Since the crack does not propagate during dynamic loading, the asymptotic representation of the fields is identical in the dynamic (Freund, 1972; Achenbach, 1972) and the static cases (Irwin, 1957) and $H(\tau)$ becomes

$$H(\tau) = \frac{1 - v^2}{E} \int_0^{\tau} K_{Id}^u(t) K_{Id}^v(\tau - t) \, \mathrm{d}t. \tag{12}$$

It can be remarked that H(τ) is a bilinear functional of two fields, say $H(\tau ; \mathbf{u}, \mathbf{v})$. Equations (10) and (12) can be combined to yield:

$$\frac{1}{2} \int_S \left\{ \mathbf{T}[\mathbf{u}] * \frac{\partial \mathbf{v}}{\partial a} - \frac{\partial \mathbf{T}[\mathbf{v}]}{\partial a} * \mathbf{u} \right\} \mathrm{d}S = \frac{1 - v^2}{E} K_{Id}^u * K_{Id}^v, \tag{13a}$$

in which time integrals have been replaced by convolution products denoted by (*) and scalar product between vectors has been implicitly assumed. In doing so, the definition of

V (11) has been explicitly included to yield (13). Therefore, both sides of (13) are expressed from now on as functions of displacement fields **u** and **v**.

Equation (13) is quite central since it relates global mechanical quantities (displacements and forces) associated with the external boundary of the solid to mechanical quantities (stress intensity factors) which characterize the crack-tip itself. In other words, it transfers (local) information which is not easily accessible to the border on which measurements can be made.

This new result can be practically applied to the determination of dynamic K_{Id}^{u} in two distinct ways:

—v(≠u) and $\partial \mathbf{v}/\partial a$ are determined either analytically or numerically. So is K_{Id}^{v} and this is done once for all for the structure to be studied and stored for later use. Equation (13) requires that **u** and **T**[**u**] be determined for the actual structure and loading conditions, say by experimental means. K_{Id}^{u} will be obtained by solving a linear convolution equation of the type :

$$A * K_{Id}^{\mathbf{u}} = H(\tau\,;\,\mathbf{u},\mathbf{v}), \quad (A \equiv K_{Id}^{\mathbf{v}}).$$ (14)

—Alternatively, one can define the auxiliary field **v** such that **v** = **u**. However determination of $\partial \mathbf{u}/\partial a$ requires at least a couple of experiments with crack lengths a and $a+\mathrm{d}a$. Here, K_{Id}^{u} will be obtained by solving a quadratic autoconvolution equation of the type :

$$K_{Id}^{\mathbf{u}} * K_{Id}^{\mathbf{u}} = H(\tau\,;\,\mathbf{u},\mathbf{u})$$ (15)

[in both cases H has been multiplied by the constant E/(1-v²)].

Before addressing practical aspects of the problem, some general remarks can be made:

—Equation (13a) is the dynamic counterpart of the static expression (Irwin, 1957) in which simple products have been replaced by convolution products to take into account dynamic aspects.

—Using Laplace transforms, Nilsson (1973) developed an expression similar to (13a). However, his expression might prove difficult to use for practical purposes since it would involve direct and inverse Laplace transforms of actual signals which are necessarily of limited duration. Such truncature will most likely affect the determination of the dynamic stress intensity.

—For arbitrary loads and geometries, (13a) can be replaced by:

$$\frac{1}{2}\int_{S}\left\{ \mathbf{T}[\mathbf{u}] * \frac{\partial \mathbf{v}}{\partial a} - \frac{\partial \mathbf{T}[\mathbf{v}]}{\partial a} * \mathbf{u} \right\}\mathrm{d}S = \frac{1-v^{2}}{E}(K_{Id}^{\mathbf{u}} * K_{Id}^{\mathbf{v}} + K_{IId}^{\mathbf{u}} * K_{IId}^{\mathbf{v}}).$$ (13b)

Mixed mode separation into pure modes I and II can be performed in this dynamic case according to the guidelines provided for the static case by Ishikawa *et al.* (1979) and Bui (1983). This is achieved by inserting into (13b) auxiliary fields v' and v^II which correspond to pure modes I and II respectively.

—Contrary to the *H*-integral, the previously defined dynamic *J*-integrals (Bui, 1978; Kishimoto *et al.*, 1980) are not pure contour integrals since they involve an area integral over the crack-tip region.

In the following sections, experimental determination of the force-displacement relationship is presented.

3. EXPERIMENTAL TECHNIQUE

The split Hopkinson bar

The split Hopkinson bar (SHB, also known as the Kolsky bar) is a convenient experimental technique to measure dynamic stresses and displacements on the faces of a compression specimen. The principle of SHB apparatus can be found in the literature (Follansbee, 1985) and will only be briefly outlined here. The basic set-up consists of a pair of long cylindrical bars (incident and transmitter), both instrumented with strain gages at their mid-length. A striker bar impacts on the incident bar, thus setting a transient compressive pulse which propagates through a small cylindrical compression cylinder sandwiched between the bars. The bars remain elastic throughout the process whereas the specimen deforms plastically. Three characteristic transient signals are recorded from the gages: the incident $\varepsilon_{in}(t)$ and reflected signals $\varepsilon_{ref}(t)$ (incident bar), and the transmitted signal $\varepsilon_{tr}(t)$ (transmitter bar) (Fig. 4). The velocities of the bar-specimen interfaces can be determined according to :

$$\begin{cases} \dot{u}_1(t) = C_L[\varepsilon_{in}(t) - \varepsilon_{ref}(t)], \\ \dot{u}_2(t) = C_L\varepsilon_{tr}(t), \end{cases} \tag{16}$$

where $\dot{u}_1$, and $\dot{u}_2$ are input (incident) and output (transmitter) velocities respectively, C_L denotes longitudinal sound velocity in the bars and t stands for time. Here, ε_{in} and ε_{tr} are compressive strains (assumed positive) whereas ε_{ref} is tensile (assumed negative). The corresponding net forces are given by :

$$\begin{cases} P_1(t) = EA[\varepsilon_{in}(t) + \varepsilon_{ref}(t)], \\ P_2(t) = EA\varepsilon_{tr}(t), \end{cases} \tag{17}$$

where E and A stand for Young's modulus and cross-sectional area of the bar respectively. All signals are actually measured at the mid-length of the bars. Due to the dispersive nature of the waves, a phase correction must be applied to each wave in order to restore its original aspect at the specimen-bar interface (Davies, 1948).
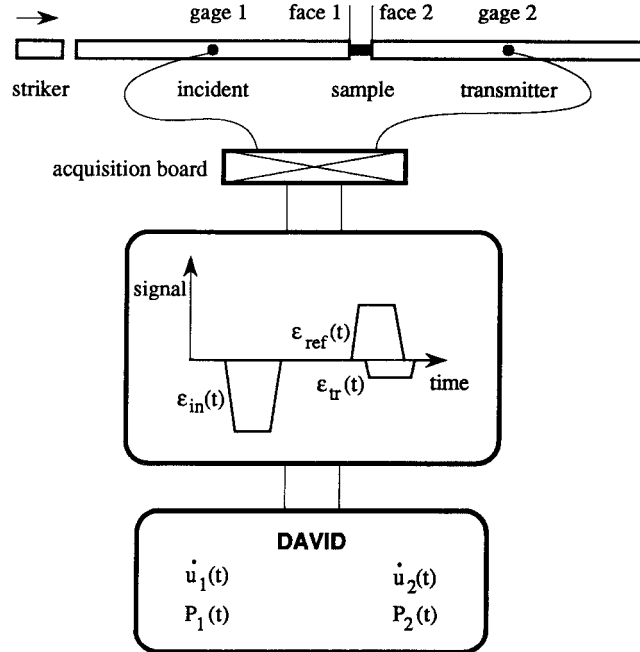

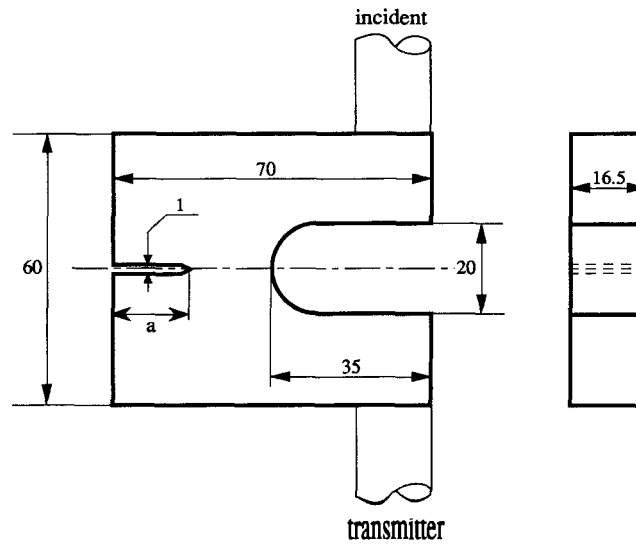Fig. 4. Split Hopkinson Bar (SHB) and signal processing apparatus.

Fig. 5. The Compact Compression Specimen (CCS) positioned between the incident and transmitter bars.

In the experiments described below, we used 1.65 x 10^{-2} m diameter-2 m length maraging steel bars. The striker, of a material and diameter identical to those of the bars, was 5 x 10^{-2} m long. The gage signals were digitized with a time step of 1 µs by means of an acquisition board and subsequently processed with DAVID software (Gary and Klepaczko, 1988) to determine stresses and velocities as a function of time at the specimenbar interfaces.

The Compact Compression Specimen (CCS)

A notched compression specimen was specially designed to fit in the SHB apparatus. This specimen, the Compact Compression Specimen (CCS), was adopted as a simple alternative to the special techniques designed to turn the SHB apparatus into a dynamic tensile facility (Duffy *et al.,* 1988). To our knowledge, the CCS is an original design which has not been used previously. The CCS is shown in Fig. 5. The dimensions quoted are by no means restrictive nor have they been optimized. However, the specimen thickness was selected so that it matches the bar diameter thus enabling two-dimensional numerical modelling. Specimens with various notch lengths were machined out of a semi-hard steel. As the branches of the specimen get closer following progression of the compressive pulse, the notch opens in a non-symmetrical way, this point being addressed later. The experiments which were performed and the reported results did not involve crack propagation and/or fracture of the specimen. The deformations remained elastic as could be ascertained both visually and by checking the specimen dimensions prior to and after impact.

4. NUMERICAL MODELLING

Two-dimensional (plane strain) dynamic finite element analysis of the CCS was carried out using CASTEM 2000 object oriented FEA code (developed by CEA-French Center for Atomic Energy). The CCS was discretized into constant strain triangles and the material model was isotropic and linear-elastic, according to the initial assumptions of an all-elastic process. Two distinct types of calculations were performed: calculations of specimens for calibration purposes and simulations of actual experiments.

Calibration specimen

Numerical modelling was carried out to provide numerical $\{\partial \mathbf{v}/\partial a; \partial \mathbf{T}[\mathbf{v}]/\partial \mathbf{a}\}$ relationships in (14) which become $\{\partial \mathbf{u}/\partial a; \partial \mathbf{T}[\mathbf{u}]/\partial a\}$ in (15). These relationships are used to validate the autodeconvolution method on the one hand, and provide calibration data to
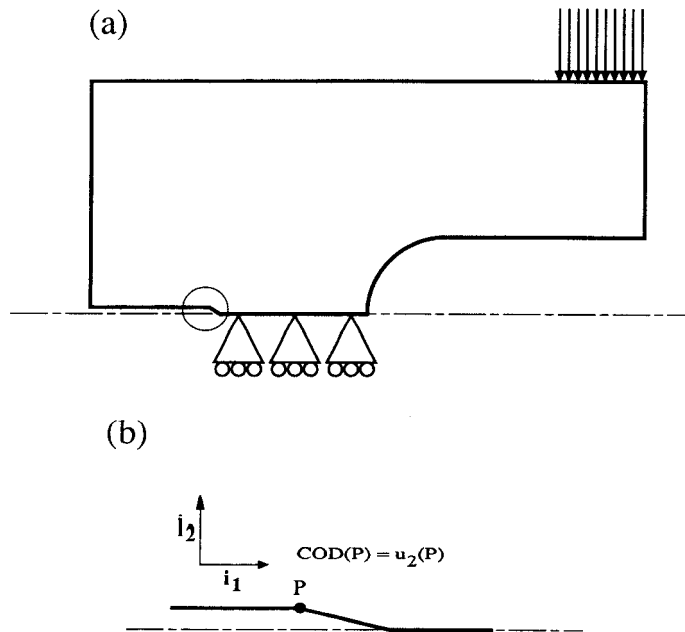
Fig. 6(a). Half the CCS used in numerical (FEM) studies for the generation of calibration data. (b) Definition of the crack opening displacement (COD).

be combined with experimental data in the linear deconvolution method on the other hand. Half the CCS was analysed and vertical displacements of the symmetry line were set to zero, this imposing symmetrical response of the specimen [Fig. 6(a)] and enforcing mode I crack opening. A Gaussian load pulse was applied to the (incident) bar-specimen interface. The pulse shape was adopted without any attempt to reproduce in detail an actual experimental pulse. The dynamic response of this interface, i.e. the velocity-force relationship was calculated by numerical integration of the equation of motion by means of the Newmark technique (Bathe, 1982). A "characteristic" interfacial velocity was defined as the vertical velocity component averaged along the contact line. It is this velocity which was used in the subsequent applications. An additional by-product of this analysis is the dynamic crack opening displacement (COD).

The COD was taken here as the vertical displacement component of the point belonging to the notch, located 2×10^{-3} m ahead and 5×10^{-4} m above the crack tip [Fig. 6(b)].

Numerical simulation of the experiment

In order to reproduce the actual SHB experiment while testing the overall modelling, the following numerical experiment was undertaken: the actual SHB with sandwiched CCS was modelled. Rigid interfacial bonding was assumed between the bars and the CCS in order to avoid the use of adjustable parameters such as contact stiffness (Mines, 1990). No boundary conditions were imposed on the displacements. The input load pulse was taken from the incident signal measured on the incident bar during an actual experiment, $\varepsilon_{in}(t)$. As it reached the incident bar-specimen interface, this pulse was part reflected part transmitted due to mechanical impedance effects. The velocity-time relationships of the two bar-specimen interfaces were calculated with the above-mentioned procedure and compared with their experimentally determined counterparts. Here too, the COD was calculated, defined this time as the difference between the vertical displacements of two symmetrically located points.

5. RESULTS AND DISCUSSION

Foreword

In this section, results will be presented for one experiment which can be considered as characteristic of the above-mentioned testing procedure. Next, on the basis of these

results, the evolution of the dynamic stress intensity factor will be calculated in a detailed procedure to illustrate the new approach. For the sake of clarity, the various results will be discussed as they are presented rather than in a separate section.

Experimental results

The following results were obtained for a CCS with a 17 x 10^{-3} m long notch. Figure 7(a) shows a typical record of the measured incident force $[P_{in}(t) = EA\varepsilon_{in}(t)]$. The resulting forces on the bar-specimen interfaces are shown in Fig. 7(b). The maximum value of $P_1(t)$ is smaller than that of $P_{in}(t)$ due to the reflected pulse. It also exceeds the maximum value of $P_2(t)$. The two peaks are shifted in time with respect to each other with very little overlapping. The transit time necessary for the pulse to travel through the CCS can be identified with the time at which pulse P_2 begins to form. From Fig. 7(b), this time is roughly equal to 55 µs. The corresponding interfacial velocities are plotted in Fig. 7(c). Here too, there is almost no overlap and the ratio of the peaks is about 0.5. It is interesting to note that the peak velocity lags behind the peak force by some 10 µs.

Numerical results

Numerical simulation of the experiment. The material constants of the bars and the specimen are listed in Table 1. The calculated interfacial velocities corresponding to the input pulse of Fig. 7(a) are shown in Fig. 8(a) in which experimental velocities have been superposed. From this figure, it can be noted that the calculated velocities are very similar to the measured ones (pulse shape, peak value and transit time), with a slight shift of the calculated transmitted velocity peak with respect to the experimental one. This shift could not be clearly identified as a numerical problem related to mesh size effects or to the material constants. It seems more likely that the observed discrepancy is related to the very nature of the interfacial contacts. Yet, despite its deliberate simplicity, this model reproduces remarkably well the salient features of the actual experiment while it also validates the hypothesis of an elastic process. The calculated corresponding COD is shown in Fig. 8(b). This result cannot be compared with its measured counterpart. However, given the accuracy of the numerical model, it is reasonable to assume that this result is equally accurate. Determination of the COD is valuable since this parameter which is not easily measurable is related to the stress intensity factor, as discussed in the next section. A general trend was noted for the maximum crack opening to occur at the time corresponding to the intersection of P_1 and P_2. Last, the various deformation stages of the CCS are visualized in Fig. 9 which shows the transient nature of the deformation as well as its lack of symmetry.

Calibration specimen. A force (F_{cal})—velocity ($\dot{v}_{cal}$) relationship was generated for a half CCS subjected to a 20 µs long-30 kN high force pulse. Two crack lengths of 16 x 10^{-3} m and 17 x 10^{-3}m were chosen for the analysis and the calculated average interfacial velocities are plotted in Fig. 10.

6. THE DETAILED PROCEDURE FOR Kid DETERMINATION

Before getting into details we can summarize the available information and its origin, as follows :

|		
Experimental	1.	Input and output forces, $P_1(t)$ and $P_2(t)$.
	2.	Input and output velocities, $\dot{v}_1(t)$ and $\dot{v}_2(t)$.
Simulated experiment	3.	Calculated input and output velocities.
	4.	Calculated COD.
Numerical Calibration	5.	Calibration force, F_{cal}.
	6.	Calibration velocity for 1st crack length (a = 16 mm).
	7.	Calibration velocity for 2nd crack length (a = 17 mm)
	8.	Calibration COD for 1st crack length (a = 16 mm).
	9.	Calibration COD for 2nd crack length (a = 17 mm).
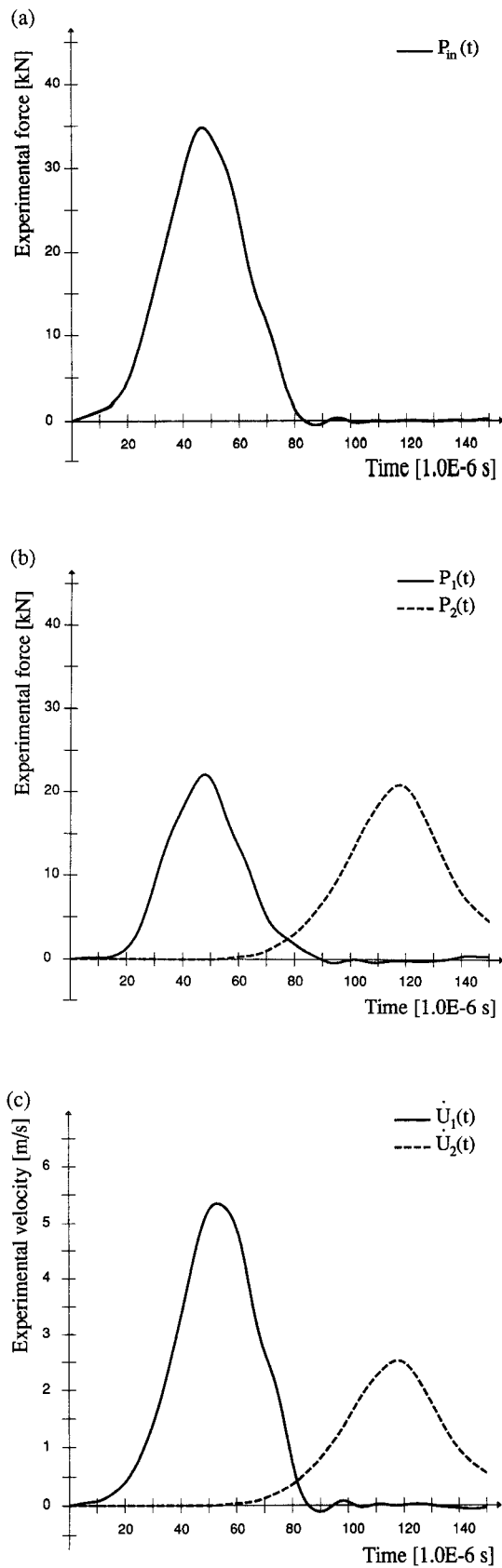
Fig. 7(a). Typical record of the experimental incident force $P_{in}(t)$ at the incident bar specimen interface. (b) Typical record of the net experimental incident $P_1(t)$ and transmitted $P_2(t)$ forces at the bar specimen interfaces. (c) Typical record of the experimental incident $\dot{u}_1(t)$ and transmitted $\dot{u}_2(t)$ velocities at the bar-specimen interfaces.

	E	υ	P
	[Pa]		[kg m-3]
Hopkinson bars	2.0 x 10"	0.250	8100
C.C.S	2.1 x 10"	0.285	7800

The autodeconvolution method

We first show the application of the quadratic autoconvolution equation (15) to K_{Id} determination on a purely numerical example in which the relevant data bears the subscript ()$_{\text{cal}}$. We use (15) with u ≡ u$_{\text{cal}}$, and K_{Id}^{u} = K_{Id}^{ucal} . For the sake of convenience the applied stress is kept constant with respect to crack length, i.e. $\partial\mathbf{T[u_{\text{cal}}]}/\partial\mathbf{a} \equiv 0$. We first evaluate the left-hand side of (13) :

$$H(\tau) = \frac{1}{2}\int_{s}\mathbf{T[u}_{cal}]*\frac{\partial\mathbf{u}_{cal}}{\partial a}\,\mathrm{d}S \tag{18}$$

where $\partial\mathbf{u}_{\text{cal}}/\partial a$ is approximated by a time integration of the difference of calibration velocities
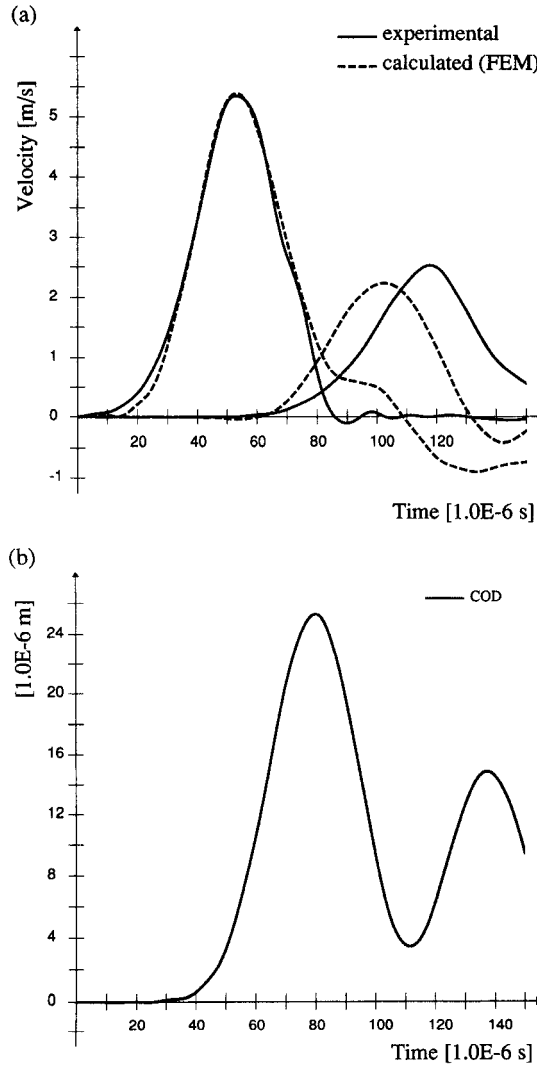

Fig. 8(a). Experimentally and numerically (FEM) determined interfacial velocities. Both curves have the same time origin. (b) Corresponding COD determined by FEM simulation.
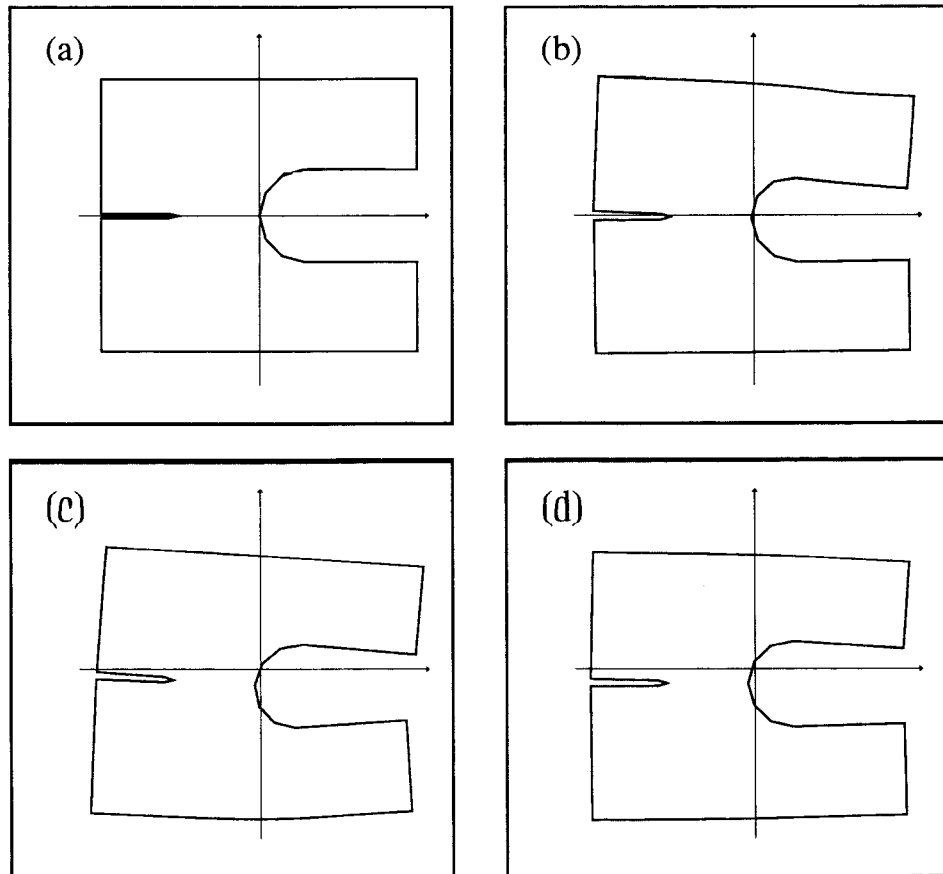
Fig. 9. FEM simulation of the experiment. Deformed CCS at time steps (a) 0, (b) 50, (c) 100, and (d) 150 μs (scaling factor for deformations 30).
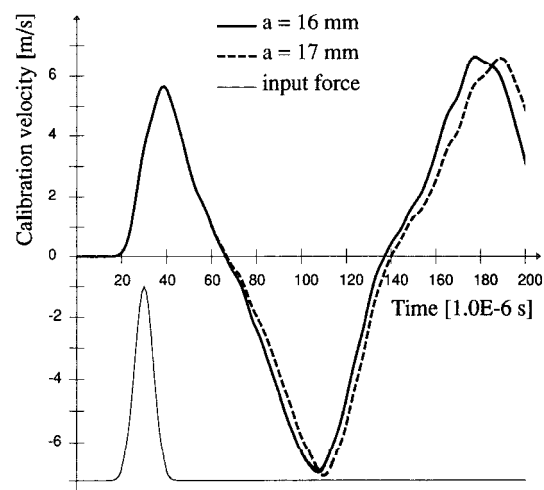

Fig. 10. Calculated (FEM) velocities for the calibration specimen with crack length 16 mm and 17 mm respectively. The input peak (fine solid line—20 μs wide and 30 kN high) is represented here in dimensionless form.
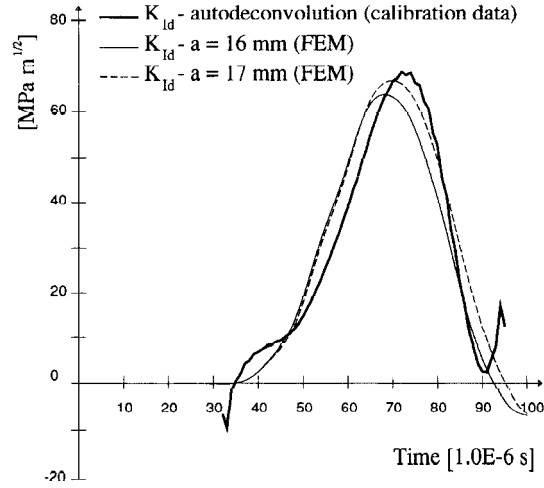
Fig. 11. Stress intensity factors $K_I(t)$. The fine line refers to $K_I(t)$ calculated (FEM) from reference data with a crack length of 16 mm. Idem for the fine dashed line and a crack length of 17 mm. The solid line refers to $K_I(t)$ calculated by autodeconvolution with calibration data.

(points 6 and 7) If $\bar{u}_{cal}$, denotes the corresponding average displacement, (18) reduces to

$$H(\tau) = F_{cal} * \frac{\partial \bar{u}_{cal}}{\partial a} = \frac{1-v^2}{E} K_{Id}^{ucal} * K_{Id}^{ucal}. \tag{19}$$

Next, the stress intensity factor is determined using the autodeconvolution procedure for $H(\tau)$ given in the Appendix. This value can be compared with the value determined directly from the calibration COD (points 8 and 9) using the well-known relationship (Irwin, 1957) :

$$COD = K_I \frac{8(1-v^2)}{E} \sqrt{\frac{r}{2\pi}}. \tag{20}$$

Typical results are shown in Fig. 11. An excellent agreement is observed between K_{Id} values obtained by two radically different procedures. This example validates the method using numerically generated data. A more concrete illustration in which actual experimental data is used is given next.

The linear deconvolution method

We now show the application of the linear convolution equation (14) to K_{Id} determination using experimental and calibration data. In this case, $\mathbf{v} = \mathbf{u}_{cal}$, and $\mathbf{u} = \mathbf{u}_{exp}$, the experimentally determined displacement field. We use the calibration value $K_{Id}^{v} = K_{Id}^{ucal}$ determined by either of the above mentioned methods (autodeconvolution or directly from calibration COD). $H(\tau)$ is calculated according to (13)

$$H(\tau) = F_{exp} * \frac{\partial \bar{u}_{cal}}{\partial a} = \frac{1-v^2}{E} K_{Id}^{uexp} * K_{Id}^{ucal}. \tag{21}$$

F_{exp} is now built with the actual forces (point 1), and it can be shown that $F_{exp} = 1/2(P_1 + P_2)$. This amounts to symmetrizing an initially non-symmetrical experiment to isolate crack-opening mode I. $K_{Id} = K_{Id}^{uexp}$ values are obtained by linear deconvolution of $H(\tau)$ (see Appendix). For comparison purposes only, we also calculated K_{Id} by applying (20) to COD
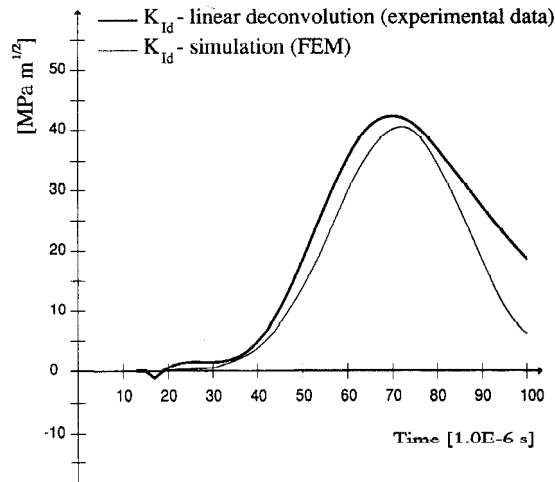
Fig. 12. Stress intensity factors $K_I(t)$. The fine line refers to $K_I(t)$ determined from the FEM simulation of the actual experiment. The fine solid line refers to $K_I(t)$ obtained by linear deconvolution with experimental data.

values (point 4) from the FEM simulation of the experiment. In Fig. 12 are plotted K_{Id} values determined by linear deconvolution and from the COD values. Here too, an excellent agreement between the two can be noted.

7. CONCLUDING REMARKS

A new method for the experimental determination of the dynamic stress intensity factor $K_{Id}(t)$ in linear-elastic materials has been developed. This method is rigorous and dynamic effects are inherently taken into account. Local crack-tip information is accessed by means of global mechanical data (forces-displacements on the specimen outer boundary) thanks to the path-independent H-integral.

This approach has been tested and validated. A specially devised experimental specimen (Compact Compression Specimen) has been used in a standard split Hopkinson bar apparatus to measure the required force-displacement relationships. Realistic numerical modelling of the experiments has also been performed.

The applicability of our approach is by no means restricted to the experimental set-up presented here. It applies equally well to any other system in which boundary forces and displacements can be measured and proper numerical modelling carried out.

Two different options for the determination of $K_{Id}(t)$ have been introduced: the autodeconvolution and the linear deconvolution methods. In the first method, two distinct experiments should be performed with slightly different crack lengths. This was carried out as a purely numerical simulation but this can also be done experimentally. In the second method, experimental results were combined with numerical (calibration) results. With both methods, $K_{Id}(t)$ was successfully obtained by solving a time convolution equation.

The outlined procedure for $K_{Id}(t)$ determination also applies to the determination of $K_{Id}(t)$ provided anti-symmetrical loads are considered in the calibration calculation. This method is relatively simple and does not require a cumbersome experimental setup or tedious repeated numerical calculations. It is quite versatile without restrictions on the type and symmetry of the imposed loads, crack opening mode, (linear elastic) material and crack geometry. The only restriction of the method is that it applies up to the instant of crack initiation but not to its subsequent propagation. It thus seems that this method can be successfully applied to a wide range of problems in the fields of fracture mechanics and materials science, including dynamic fracture toughness determination.

REFERENCES

Achenbach, J. D. (1972). Dynamic effects in brittle fracture. In *Mechanics Today* (Edited by S. Nemat Nasser), Vol. 1, pp. 1-57.

Bathe, K. J. (1982). *Finite Element Procedures in Engineering Analysis.* Prentice-Hall, Englewood Cliffs, NJ.

Beinert, J. and Kalthoff, J. F. (1981). Experimental determination of dynamic stress intensity factors by shadow patterns. In *Mechanics of Fracture* (Edited by G. C. Sih), Vol. 7, pp. 281-330. Martinus Nijhoff, Dordrecht.

Bui, H. D. (1978). *Mécanique de la Rupture Fragile.* Masson, Paris.

Bui, H. D. (1983). Associated path independent *J*-integrals for separating mixed modes. *J. Mech. Phys. Solids* **31**(6), 439-448.

Bui, H. D. and Maigre, H. (1988). Facteur d'intensité dynamique des contraintes tiré des grandeurs mécaniques globales. *C. R. Acad. Sc. Paris* **t. 306**, Serie II, 1213-1216.

Davies, R. M. (1948). A critical study of the Hopkinson pressure bar. *Phil. Trans. R. Soc. London* **Series A** (240), 378-457.

Duffy, J., Suresh, S., Cho, K. and Bopp, E. R. (1988). A method for dynamic fracture initiation testing of ceramics. *ASME J. Engng Mater. Tech.* **110**, (October).

Follansbee, P. S. (1985). *The Hopkinson bar, ASM. Metals Handbook, Vol.* 9 (9th edn.). Metals Park, OH.

Freund, L. B, (1972). Energy flux into the tip of an extending crack in an elastic solid. J. *Elasticity 2(4),* 341-349.

Gary, G, and Klepaczko, J. R, (1988). DAVID, Logiciel de dépouillement de l'essai de compression par barres de Hopkinson. Ecole Polvtechnique-Universite de Metz.

Irwin, G. R. (1957). Analysis of stresses and strains near the end of a crack traversing a plate. *J. Appl. Mech.* **24**(3), 361-364.

Ishikawa, H., Kitagawa, H. and Okamura, H. (1979). *J* integral of a mixed mode crack and its application. In *Mechanical Behaviour of Materials* (Edited by K. J. Miller and R. F. Smith), pp. 447-455. Pergamon Press, Oxford.

Kishimoto, K., Aoki, S. and Sakata, M. (1980). On the path-independent integral. *J. Engng Fract. Mech.* **13**, 841-850.

Kobayashi, A. S. (1987). *Handbook on Experimental Mechanics.* Prentice-Hall, Englewood Cliffs, NJ.

Maigre, H. (1990). Contribution théorique à 1'identification des grandeurs caracteristiques en mécanique de la rupture dynamique. Doctoral Thesis. Ecole Polyteclinique, Palaiseau.

Mall, S., Kobayashi, A. S. and Loss, F. J. (1980). Dynamic fracture analysis of notched bend specimen. In *Crack Arrest Methodology and Applications* (Edited by G. T. Hahn and M. F. Kanninen), pp. 70-85. ASTM STP711, Philadelphia, PA.

Manogg, P. (1966). Investigation of the rupture of a plexiglass plate by means of an optical method involving high speed filming and shadow optical around holes drilled in the plate. *Int. J. Fract. Mech.* **2**, 604-613.

Mines, R. A. W. (1990). Characterization and measurement of the mode I dynamic initiation of cracks in metals at intermediate strain rates-a review. *Int.* J. *Impact Engng* **9**(4), 441-454.

Nilsson, F. (1973). A path-independent integral for transient crack problems. *Int. J. Solids Structures* **9**, 1107-1115.

Rice, J. R. (1968). A path-independent integral and the approximate analysis of strain concentration by notches and cracks. *J. Appl. Mech.* **35**, 379-386.

Schwartz, L. (1979). *Méthodes Mathématiques pour les Sciences Physiques.* Hermann, Paris.

Theocaris, P. S. (1981). Elastic stress intensity factors evaluated by caustics. In *Mechanics of Fracture* (Edited by G. C. Sih), Vol. 7, pp. 189-252. ASME, New York, NY.

Tikhonov, A. and Arsenine, V. (1976). *Méthode de Résolution de Problèmes Mal-Posés.* Mir, Moscow.

Yang, K. H., Kobayashi, A. S. and Emery, A. F. (1988). Dynamic fracture characterization of ceramic matrix composites. *J. Phys. Colloque* C3 **Suppt. 9**(49), 223-236.

APPENDIX

An algorithm for solving eqns (14) *and* (15)

It is well established that the convolution equation $A * X = H$ admits no solution except for particular "compatible" couples (A, H). It is also known that such an equation is quite unstable with respect to A and H. In other words, if X exists as a solution, it can be perturbed by an arbitrary value ΔX and yet ($X + \Delta X$) is also almost a solution, that is $A * (X + \Delta X) \approx H$ (Schwartz, 1979; Tikhonov and Arsenine, 1976)_ The above-mentioned applies to the less "classical" equation $X * X = H$.

In the present case, A and H are not arbitrary. Rather, they are generated by a physical problem, a fact which ensures "compatibility". We also know that a solution X must exist. Since X is now the dynamic stress intensity factor, one can reasonably speculate that the shape of this solution will somehow be similar to the shape of the loading pulse with the same degree of regularity. Furthermore, we deal here with discrete datapoints digitized in time either numerically or experimentally. Consequently, (14) and (15) are discretized as:

$$\sum_{p=0}^{n} A_{n-p} X_p = H_n \text{ and } \sum_{p=0}^{n} X_{n-p} X_p = H_n \text{ , respectively.}$$

However, it can be shown that direct inversion of these triangular systems leads to highly oscillatory solutions in contradiction with the physical character of the solution (Maigre, 1990).

Therefore, to stabilize the solution, a best-fit is obtained by adding to the problem the constraint that the solution built from the even order terms should be as close as possible to that obtained from the odd order terms. Determination of a physically sound solution now becomes a minimization problem with constraints.